



Short communication

Oxidation and electrical behavior of ferritic stainless steel interconnect with Fe–Co–Ni coating by electroplating

Shujiang Geng ^{a,b,*}, Shaojun Qi ^a, Dong Xiang ^a, Shenglong Zhu ^b, Fuhui Wang ^b

^a School of Materials and Metallurgy, Box 119, Northeastern University, 3-11 Wenhua Road, Shenyang 110819, China

^b State Key Laboratory for Corrosion and Protection, Institute of Metal Research, Chinese Academy of Sciences, 62 Wencui Road, Shenyang 110016, China

HIGHLIGHTS

- Fe–Co–Ni coating has been electroplated on ferritic stainless steel.
- $(\text{Fe},\text{Co},\text{Ni})_3\text{O}_4$ spinel atop Cr_2O_3 was thermally grown on the steel with coating.
- The double-layer surface scale exhibited a high electrical conductivity.
- $(\text{Fe},\text{Co},\text{Ni})_3\text{O}_4$ outer layer acted as an effective barrier to Cr outward migration.
- $(\text{Fe},\text{Co},\text{Ni})_3\text{O}_4$ outer layer reduced the growth of the Cr_2O_3 inner layer.

ARTICLE INFO

Article history:

Received 13 February 2012

Received in revised form

6 May 2012

Accepted 7 May 2012

Available online 12 May 2012

Keywords:

Solid oxide fuel cell

Electroplated Fe–Co–Ni coating

Interconnect

Oxidation

Area specific resistance

ABSTRACT

Fe–Co–Ni coating is deposited on ferritic stainless steel using a cost-effective technique of electroplating for intermediate-temperature solid oxide fuel cell (SOFC) interconnects application. The steel with Fe–Co–Ni coating has been evaluated in air at 800 °C corresponding to the cathode environment of SOFC. The results indicate that the steel with Fe–Co–Ni coating experiences an initially large mass gain, and then the mass gain increases slightly after the first-week rapid oxidation stage. After thermal exposure in air at 800 °C, the Fe–Co–Ni coating has been converted into $(\text{Fe},\text{Co},\text{Ni})_3\text{O}_4$ spinel layer underneath which a Cr_2O_3 layer is developed from the steel substrate. The outer layer of $(\text{Fe},\text{Co},\text{Ni})_3\text{O}_4$ spinel has not only suppressed Cr migration outward but also reduced the growth rate of the inner layer of Cr_2O_3 . The steel with Fe–Co–Ni coating exhibits a stable surface oxide scale area specific resistance (ASR) which is much lower than that of the bare steel. $(\text{Fe},\text{Co},\text{Ni})_3\text{O}_4$ spinel is a promising protective coating for SOFC steel interconnect.

© 2012 Elsevier B.V. All rights reserved.

1. Introduction

The development of intermediate-temperature solid oxide fuel cells (SOFCs) which are operating at or below 800 °C [1–4] has made it possible to use high temperature oxidation resistant alloys as interconnect materials in the SOFC stacks to supplant the conventional LaCrO_3 -based ceramics. Chromia-forming ferritic stainless steels (FSS) have been considered among the most promising candidates for SOFC interconnect applications due to their good oxidation resistance as well as acceptable electrically conductive oxide scale, good mechanical properties, low cost and appropriate thermal expansion behavior [5–10]. However, there

are challenges associated with FSS, including increasing electrical resistance originated from the chromia growth over time, and the migration of Cr via Cr_2O_3 evaporation. These volatile Cr species can migrate to and poison the cathode or the interface between cathode and electrolyte [11,12], subsequently leading to the degradation in cell performance [13–18].

To overcome the problems above, it is very important to develop coatings on FSS particularly at the cathode side of SOFC. Accordingly, the candidate materials for the coatings should be an effective barrier to the oxygen inward diffusion and/or the chromium outward diffusion in order to reduce the growth rate and evaporation of chromia formed on FSS, and be also required to have a high electrical conductivity as well as good thermal expansion match with the substrate steel and be thermal chemically stable and compatible to adjacent stack components in SOFC stack [19].

With this in mind, a variety of coatings such as conductive perovskites [19–22] and spinels [23–25] have been explored as

* Corresponding author. School of Materials and Metallurgy, Box 119, Northeastern University, 3-11 Wenhua Road, Shenyang 110819, China. Tel.: +86 24 83673860; fax: +86 24 83687731.

E-mail address: gengsj@smm.neu.edu.cn (S. Geng).

barrier to hinder the evaporation of chromia. The techniques used for coatings on FSS include sol–gel method [26,27], chemical vapor deposition [28,29], plasma spraying [30], slurry coating [31] and magnetron sputtering [32]. Recently, electrodeposition of metal or alloy coatings followed by subsequent thermal exposure to form spinel coatings directly on the FSS substrates has been considered as an economical and simple technique [33–36] due to its advantages such as better coating-to-substrate adhesion, denser, less porous spinel coatings and good coverage of the electro-deposited coating on almost any substrate surfaces especially for complex-shaped interconnects. Moreover, the thickness of the final spinel coating can be readily controlled by adjusting the electrodeposition parameters including cathode current density and time [37].

In our previous work, $(\text{Fe},\text{Co},\text{Ni})_3\text{O}_4$ spinel outer layer thermally grown on Fe–Co–Ni alloy with low content of Cr in SOFC cathode environment had a high electrical conductivity and CTE match with other cell components, and reduced the growth rate and evaporation of the Cr_2O_3 inner layer [38]. In addition, the standard electrode potential of Fe^{2+}/Fe ($-0.44V_{\text{SCE}}$) is relatively close to those of Co^{2+}/Co ($-0.28V_{\text{SCE}}$) and Ni^{2+}/Ni ($-0.25V_{\text{SCE}}$). Therefore, co-deposition of Fe–Co–Ni coating via electroplating is feasible and the composition of deposited Fe–Co–Ni coating might be easily controlled by adjusting the concentration of metal cations (Fe^{2+} , Co^{2+} and Ni^{2+}) in the electroplating solution.

Our aim is to electroplate Fe–Co–Ni coating on ferritic stainless steel, followed by oxidation in SOFC cathode operating environment. The Fe–Co–Ni coating is highly expected to be thermally converted into a $(\text{Fe},\text{Co},\text{Ni})_3\text{O}_4$ spinel outer layer atop a protective Cr_2O_3 inner layer developed from the steel substrate. The present work focuses on evaluation of the oxidation behavior and surface scale electrical properties of the electroplated Fe–Co–Ni coating applied to ferritic stainless steel in air at 800 °C.

2. Experimental

Pieces (15×10 mm) were cut from 1 mm thick ferritic stainless steel sheet (nominal weight percent: 16.4% Cr, 0.28% Si, 0.13% Mn, 0.005% P, 0.005% C, 0.004% S, and the balance Fe) by electric-discharge machining (EDM). After drilling a 1.5-mm diameter hole in the upper center, each piece was ground to 1000 grits with SiC sand paper, ultrasonically cleaned in acetone, followed by rinsing in alkaline and acid solutions, respectively, and then electroplated in the solution with pH value adjusted to 4.5, containing 40 g L^{-1} $\text{NiSO}_4 \cdot 6\text{H}_2\text{O}$, 10 g L^{-1} $\text{NiCl}_2 \cdot 6\text{H}_2\text{O}$, 10 g L^{-1} $\text{FeSO}_4 \cdot 7\text{H}_2\text{O}$, 10 g L^{-1} $\text{CoSO}_4 \cdot 7\text{H}_2\text{O}$ and 15 g L^{-1} H_3BO_3 . The stainless steel substrate was used as the cathode and nickel plate was used as the anode. The experimental procedure was carried out as described in our previous work [39]. Fe–Co–Ni coating was electroplated at 55 °C under a cathode current density of 27 mA cm^{-2} for 5 min.

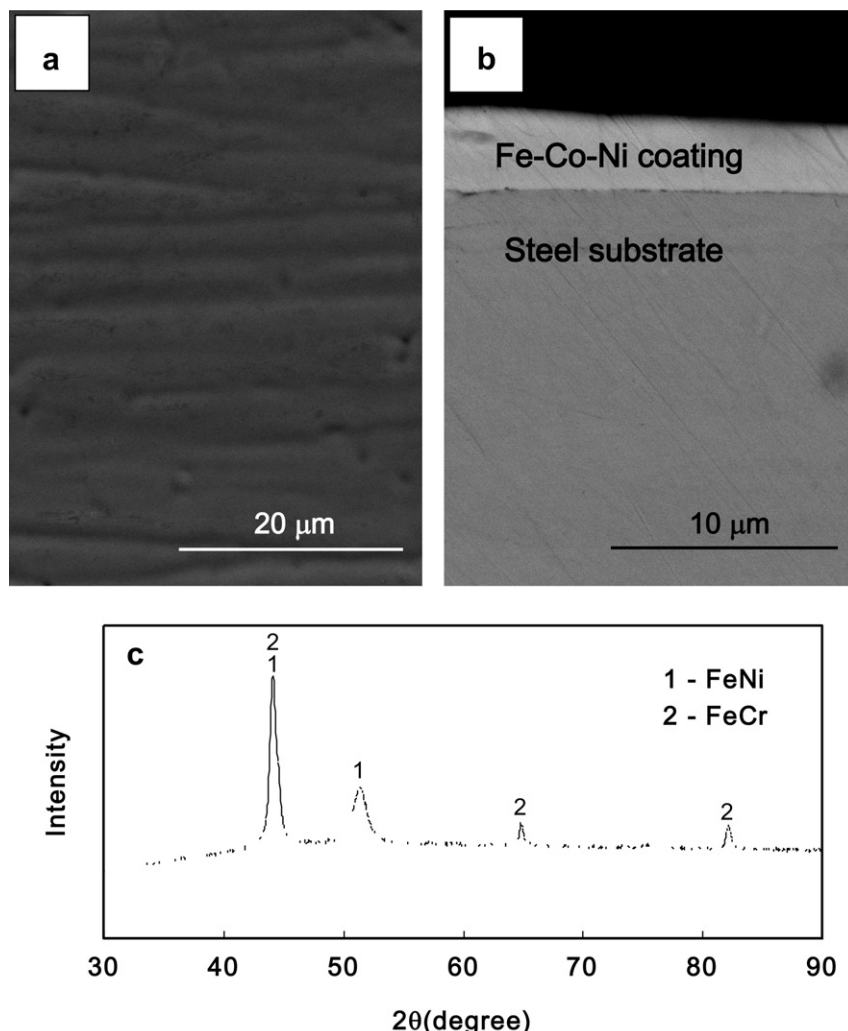


Fig. 1. SEM surface (a) and cross-sectional (b) images and XRD pattern (c) of the steel with Fe–Co–Ni coating.

Oxidation testing of the steel with Fe–Co–Ni coating was carried out in a box furnace. The samples were hung in alumina crucibles, oxidized at 800 °C in air for totally three weeks. The weight of each sample was measured after furnace cooling to room temperature following each 1-week thermal exposure. The phase structure of the oxide scales formed on the sample was identified with X-ray diffraction (XRD). The surface morphologies and cross-sections of the oxidized samples were observed using scanning electron microscopy (SEM) with an energy dispersive X-ray spectroscopy (EDX).

Electrical resistance of oxidized samples was measured using 4-point method in air at 800 °C. The measurement apparatus was designed as shown in our previous paper [35]. Two of the oxidized surfaces were covered with Pt paste. Each Pt foil had two welded Pt leads. Two alumina rods and springs were used to apply pressure and clamp the assembly together during measurement. One pair of leads was used to apply a constant current and the other pair was for voltage measurement. A constant current of 10 mA was used in the measurement reported in this paper. The resistance (R) was calculated according to the Ohm's law, $R = V/2I$. The area specific resistance (ASR) of the oxide scales which reflected both the electrical conductivity and the thickness of the oxide scale was then equal to R multiplied by the area that the Pt paste covered.

3. Results and discussion

3.1. Morphologies, composition and structure of as-electroplated coating

Fig. 1 is showing surface/section morphologies and XRD patterns of the ferritic stainless steel with electroplated coating. **Fig. 1a** shows an SEM image of the surface of an as-electroplated Fe–Co–Ni coating. The lines observed on the surface were grinding marks present underneath the coating from the preparation of the steel substrate before electroplating. The cross-section morphology of the steel with Fe–Co–Ni coating is shown in **Fig. 1b**. The electroplated Fe–Co–Ni coating was continuous and dense with a thickness around 3–4 μm, and exhibited a good-bonding to the steel substrate. Analysis by EDX demonstrated that Fe, Co and Ni contents (atomic percent) in the coating were 25%, 20.6% and 54.4%, respectively, indicating the electroplated coating contained Fe, Co and Ni. **Fig. 1c** shows XRD patterns of the steel with Fe–Co–Ni coating. Diffraction peaks consisted of Fe–Ni

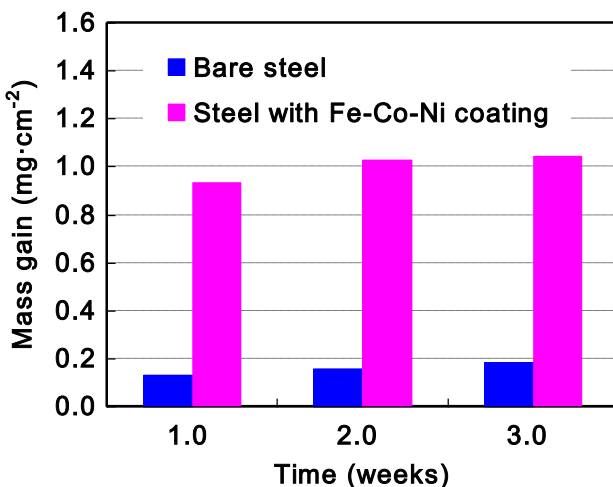


Fig. 2. Oxidation mass gains of the bare steel and the steel with Fe–Co–Ni coating in air at 800 °C.

and Fe–Cr phases were present. Fe–Ni phase should be originated from the electroplated coating. It is evident that no phases containing Co has been detected. However, Co was detected in the coating from EDX analysis. This is most likely due to the formation of a solid solution of Co present in Fe–Ni phase. Obviously, Fe–Cr phase was detected from steel substrate, as the coating was not thick enough to block X-ray penetration. From the results combined EDX and XRD, it can be confirmed that the Fe–Co–Ni coating has been electroplated on the steel.

3.2. Oxidation behaviors

The mass gain of the samples after oxidation in air at 800 °C is shown in **Fig. 2**. For the bare steel, the mass gain increased slightly with oxidation time due to the formation of the protective Cr₂O₃ scale, consistent with our previous work [35]. However, the mass gain of the steel with Fe–Co–Ni coating was much higher than that of the bare steel. The high mass gain of the steel with coating should be resulted from the oxidation of the Fe–Co–Ni coating electroplated on the steel. Conspicuously, after the first-week rapid oxidation, the mass gain of the steel with the electroplated coating increased insignificantly with oxidation time, and its oxidation rate was similar to that of the bare steel, which implied that a protective

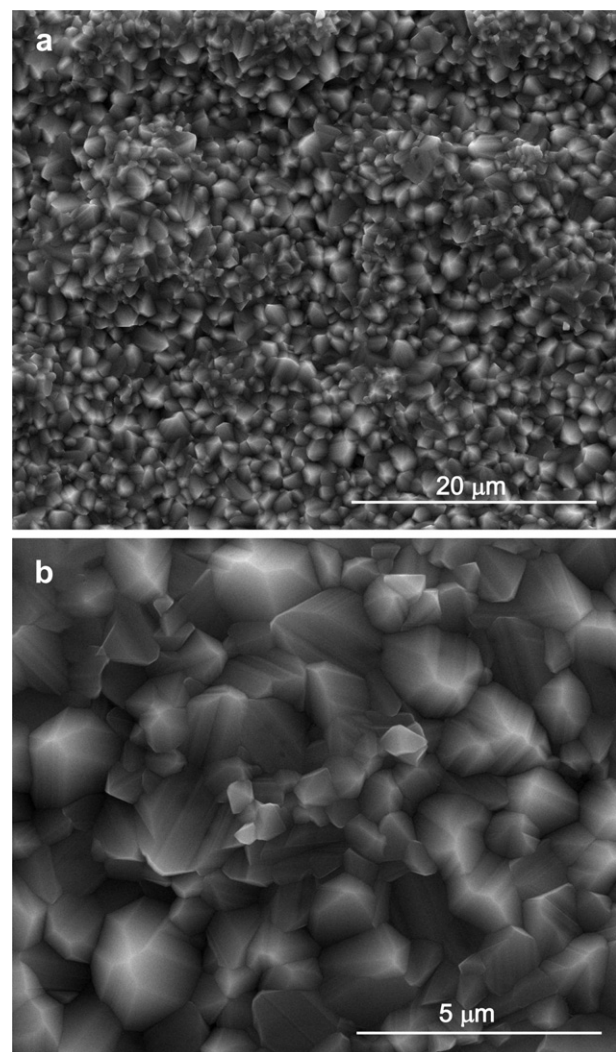


Fig. 3. Surface morphologies of the steel with Fe–Co–Ni coating after oxidation for 3 weeks in air at 800 °C.

oxide layer has been formed on the steel with coating after the rapid mass gain during the earlier stage.

Fig. 3 shows the surface morphologies of the steel with Fe–Co–Ni coating after 3-week oxidation in air at 800 °C. Fig. 3a and b are showing a lower and higher magnitude images, respectively. The surface of the steel with Fe–Co–Ni coating was covered with uniform and dense oxide crystals, which was completely different from that of the bare steel after oxidation of 3-week in the identical condition. In addition, no spallation or cracks were observed on the oxidized surface of the steel with this electroplated coating compared to that of the bare steel [35].

It is shown in Fig. 4 that the cross-sectional images with EDX elements line scan of the bare steel and the steel with Fe–Co–Ni coating after a 3-week thermal exposure in air at 800 °C. In case of the steel with coating, as shown in Fig. 4b, the surface oxide scale

was comprised of a double-layer oxide structure with an outer Cr-free layer and an inner Cr-rich layer. The outer layer of the oxide scale was rich in Fe, Co and Ni, and no Cr was detected. The inner layer was Cr-rich oxide with small amount of Mn. Nevertheless, the surface scale thermally grown on the bare steel consisted of Cr-rich oxide with small amount of Mn-rich oxide on the outer surface, as demonstrated in Fig. 4a, consistent with previous study [35]. This also confirmed that the composition of the surface oxide scale formed on the steel with Fe–Co–Ni coating was completely different from that on the bare steel.

Fig. 5 presents XRD patterns for oxidized coupons in air at 800 °C. The oxide scale formed on the bare steel after a 3-week oxidation consisted of Cr_2O_3 and $(\text{Mn},\text{Cr})_3\text{O}_4$ [35]. In contrast, $(\text{Fe},\text{Co},\text{Ni})_3\text{O}_4$ spinel and Cr_2O_3 were thermally grown on the steel with Fe–Co–Ni coating after thermal exposure under identical test condition. From the combined evidences of XRD (Fig. 5) and EDX (Fig. 4b), the outer oxide layer rich in Fe, Co and Ni was $(\text{Fe},\text{Co},\text{Ni})_3\text{O}_4$ spinel which was thermally converted from the electroplated Fe–Co–Ni coating, and the inner oxide layer rich in Cr was Cr_2O_3 developed from the steel substrate. It was the formation of the protective inner Cr_2O_3 layer that lowered oxidation rate of the steel with Fe–Co–Ni coating after the first-week rapid oxidation, consistent with the mass gain as shown in Fig. 2.

It can be seen in Fig. 4b that the outer $(\text{Fe},\text{Co},\text{Ni})_3\text{O}_4$ spinel layer is dense and well bonded to the inner Cr_2O_3 layer. Moreover, the whole surface oxide scale adhesion to the steel substrate seemed to be strong. As shown in Fig. 4a, the Cr_2O_3 layer with an around 2.0 μm thickness was formed on the bare steel after 3-week oxidation. However, the inner Cr_2O_3 layer developed on the steel with Fe–Co–Ni coating (Fig. 4b) was only about 1.0 μm which was a 2-fold decrease in thickness as compared to the former, indicating that the formation of the outer $(\text{Fe},\text{Co},\text{Ni})_3\text{O}_4$ spinel layer did reduce the growth rate of the inner Cr_2O_3 layer. It is evidently implied that the outer $(\text{Fe},\text{Co},\text{Ni})_3\text{O}_4$ spinel layer not only has blocked Cr outward migration, but also has suppressed oxygen inward diffusion, subsequently leading to the lower growth rate of the inner Cr_2O_3 layer on the steel with the electroplated Fe–Co–Ni coating.

3.3. Electrical properties of thermally grown oxide scale

After oxidation in air at 800 °C for 3 weeks, the ASR of the oxidized coupons was measured. Fig. 6 shows the surface scale ASR

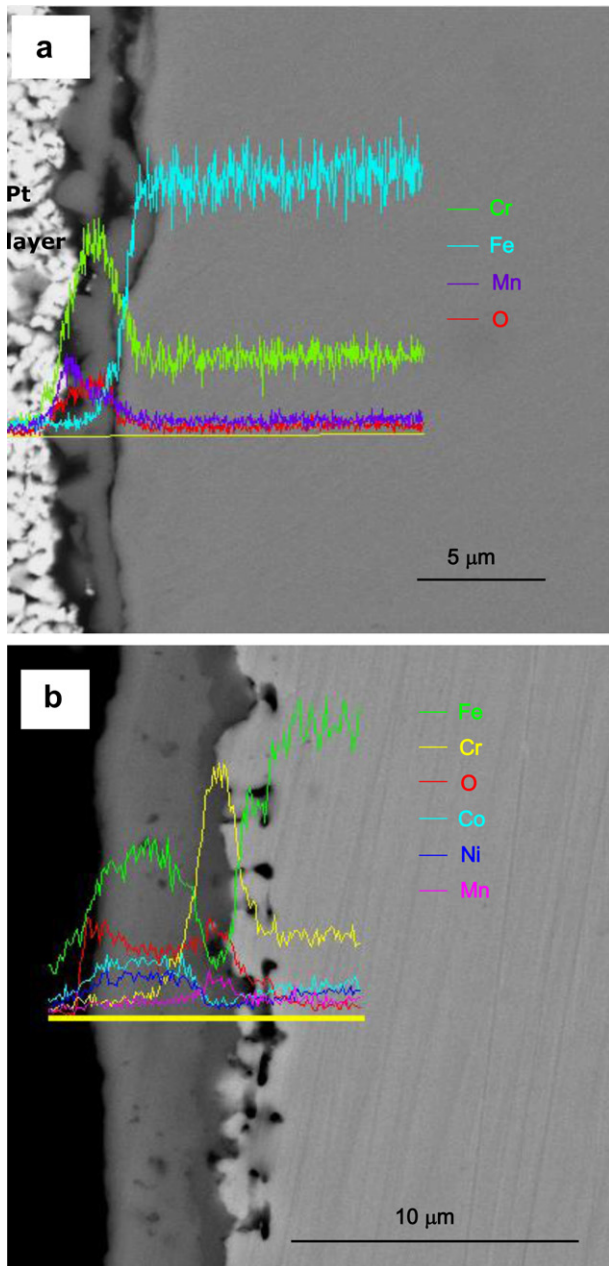


Fig. 4. Cross-sectional morphologies with elements line scan of the bare steel (a) and the steel with Fe–Co–Ni coating (b) after oxidation for 3 weeks in air at 800 °C.

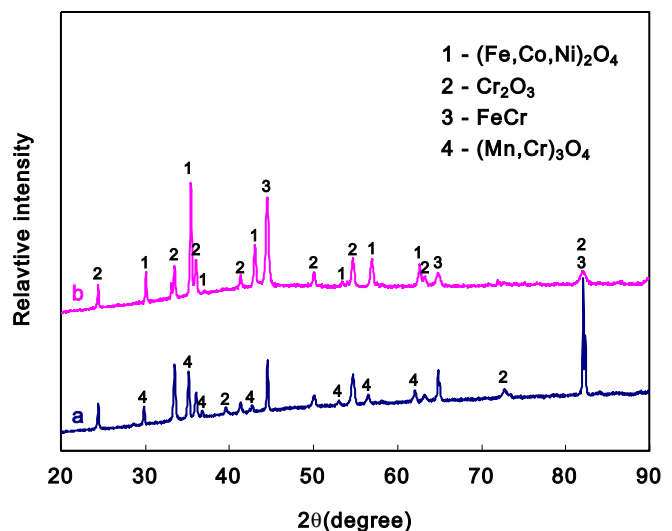


Fig. 5. XRD patterns of the bare steel (a) and the steel with Fe–Co–Ni coating (b) after oxidation for 3 weeks in air at 800 °C.

of the steel with Fe–Co–Ni coating as a function of time in air at 800 °C, in comparison with that of the bare steel under the same test condition. Apparently, the scale ASR of the bare steel increased with time, and was higher than that of the steel with Fe–Co–Ni coating, although the oxide scale (around 2.0 μm thick) developed on the bare steel was thinner than that (around 5.0 μm thick) formed on the steel with the electroplated coating. In addition, during the initial 2 h, the scale ASR for the steel with Fe–Co–Ni coating exhibited a slight decrease, most likely due to the contact problem between the Pt paste and sample, and then it remained stable, almost no change with the testing time.

The lower scale ASR for the steel with Fe–Co–Ni coating over the bare steel is related to the different surface oxide structures developed on them. As shown in Fig. 4, the oxide scale formed on the steel with Fe–Co–Ni coating was composed of a (Fe,Co,Ni)₃O₄ spinel outer layer and a thin Cr₂O₃ inner layer after oxidation in air at 800 °C. However, a Cr₂O₃ layer with small amount of (Mn,Cr)₃O₄ was grown on the bare steel upon the same thermal exposure. The lower scale ASR for the steel with the electroplated coating can be attributed to the higher electrical conductivity of (Fe,Co,Ni)₃O₄ spinel [38] compared to Cr₂O₃ and (Mn,Cr)₃O₄, subsequently reducing the contact resistance between the Pt current collector and (Fe,Co,Ni)₃O₄ compared to between Cr₂O₃/(Mn,Cr)₃O₄ and Pt. Furthermore, the Cr₂O₃ layer formed on the steel with Fe–Co–Ni coating was thinner than that on the bare steel, which also contributed to the lower surface scale ASR. The stable scale ASR of the steel with Fe–Co–Ni coating further confirmed that the growth of the Cr₂O₃ layer formed on the steel with the electroplated coating was lower than that on the bare steel. In addition, it is possible that the lower scale ASR for the steel with Fe–Co–Ni coating is in part resulted from the doping of Ni and/or Co in the Cr₂O₃ inner layer, which needs further study to verify.

Based on those results above, the (Fe,Co,Ni)₃O₄ spinel layer thermally converted from the electroplated Fe–Co–Ni coating is a promising candidate as Cr-free coatings on ferritic stainless steel interconnect for intermediate-temperature SOFC, as the Cr-free (Fe,Co,Ni)₃O₄ spinel outer layer not only had a high electrically conductivity, but also suppressed the Cr evaporation and reduced the growth rate of the Cr₂O₃ inner layer developed from steel substrate.

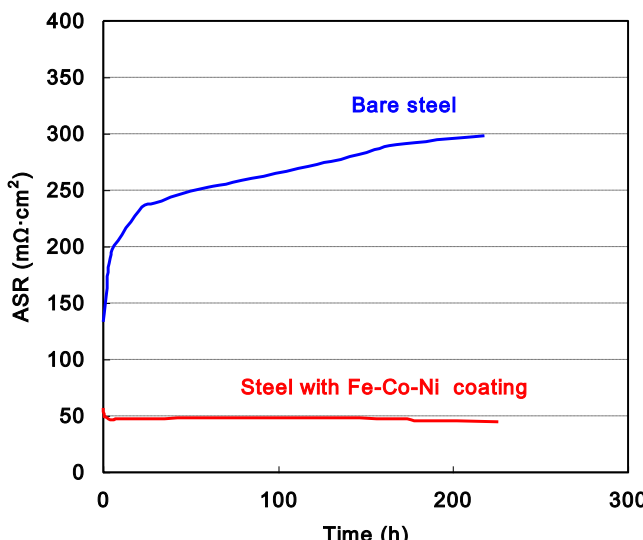


Fig. 6. Surface scale ASR of the steel with Fe–Co–Ni coating after 3-week oxidation as a function of time in air at 800 °C, in comparison with that of the bare steel under the same test condition.

4. Conclusion

A double-layer oxide scale with an electrically conductive, Cr-free (Fe,Co,Ni)₃O₄ spinel outer layer and a protective Cr₂O₃ inner layer was thermally converted on the steel with the electroplated Fe–Co–Ni coating in air at 800 °C. The (Fe,Co,Ni)₃O₄ spinel outer layer not only suppressed the evaporation of the Cr₂O₃ inner layer, but also reduced the growth rate of the Cr₂O₃ inner layer and improved the electrical performance of the whole surface scale.

Acknowledgements

This research was sponsored by the National Key Basic Research Program of China (973 Program, No. 2012CB625102) and the Fundamental Research Funds for the Central Universities (Grant No. N110402001).

References

- [1] S. de Souza, S.J. Visco, L.C. De Jonghe, J. Electrochem. Soc. 144 (1997) L35–L37.
- [2] T. Ishihara, H. Matsuda, Y. Takita, J. Am. Chem. Soc. 116 (1994) 3801–3803.
- [3] P. Huang, A. Petric, J. Electrochem. Soc. 143 (1996) 1644–1648.
- [4] K. Huang, R.S. Tichy, J.B. Goodenough, J. Am. Ceram. Soc. 81 (1998) 2565–2575.
- [5] M. Dokuya, Solid State Ionics 152 (2002) 383–392.
- [6] Z. Yang, J.S. hardy, M.S. Walker, G. Xia, S.P. Simmer, J.W. Stevenson, J. Electrochem. Soc. 151 (2004) A1825–A1831.
- [7] J. Pu, J. Li, B. Hua, G. Xie, J. Power Sources 158 (2006) 354–360.
- [8] M. Han, S. Peng, Z. Wang, Z. Yang, X. Chen, J. Power Sources 164 (2007) 278–283.
- [9] S. Geng, J. Zhu, J. Power Sources 160 (2006) 1009–1016.
- [10] S. Geng, J. Zhu, Z. Lu, Script Mater 55 (2006) 239–242.
- [11] S.P.S. Badwal, R. Deller, K. Fogler, Y. Ramprakash, J.P. Zhang, Solid State Ionics 99 (1997) 297–310.
- [12] Y. Matsuzaki, I. Yasuda, Solid State Ionics 132 (2000) 271–278.
- [13] K. Hilpert, D. Das, M. Miller, D.H. Peck, R. Weiβ, J. Electrochem. Soc. 143 (1996) 3642–3647.
- [14] S.C. Paulson, V.I. Birss, J. Electrochem. Soc. 151 (2004) A1961–1968.
- [15] S. Taniguchi, M. Kadowaki, H. Kawamura, T. Yasuo, Y. Akiyama, Y. Miyaki, T. Saitoh, J. Power Sources 55 (1995) 73–79.
- [16] Y. Matsuzaki, I. Yasuda, J. Electrochem. Soc. 148 (2001) A126–A131.
- [17] J.Y. Kim, V.L. Sprengle, N.L. Canfield, K.D. Meinhardt, L.A. Chick, J. Electrochem. Soc. 153 (2006) A880–A886.
- [18] S. Jiang, J. Zhang, X. Zheng, J. Eur. Ceram. Soc. 22 (2002) 361–373.
- [19] Z. Yang, G. Xia, G.D. Maupin, J.W. Stevenson, Surf. Coat. Technol. 201 (2006) 4476–4483.
- [20] J.H. Kim, R.H. Song, S.H. Hyun, Solid State Ionics 174 (2004) 185–191.
- [21] X. Montero, N. Jordan, J. Piron-Abellán, F. Tietz, D. Stover, M. Cassir, I. Villarreal, J. Electrochem. Soc. 156 (2009) B188–B196.
- [22] Z. Yang, G. Xia, G.D. Maupin, J.W. Stevenson, J. Electrochem. Soc. 153 (2006) A1852–A1858.
- [23] A. Petric, H. Ling, J. Am. Ceram. Soc. 90 (2007) 1515–1520.
- [24] X. Montero, F. Tietz, D. Sebold, H.R. Buchkremer, A. Ringue, M. Cassir, A. Laresgoiti, I. Villarreal, J. Power Sources 184 (2008) 172–179.
- [25] Z. Yang, G. Xia, S.P. Simmer, J.W. Stevenson, J. Electrochem. Soc. 152 (2005) A1896–A1901.
- [26] B. Hua, J. Pu, W. Gong, J. Zhang, F. Lu, J. Li, J. Power Sources 185 (2008) 419–422.
- [27] W. Qu, H. Li, D. G.Ivey, J. Power Sources 138 (2004) 162–173.
- [28] S. Fontana, R. Amendola, S. Chevalier, P. Piccardo, G. Caboche, M. Viviani, R. Molins, M. Sennour, J. Power Sources 171 (2007) 652–662.
- [29] G. Cabour, G. Caboche, S. Chevalier, R. Piccardo, J. Power Sources 156 (2006) 39–44.
- [30] D.P. Lim, D.S. Lim, J.S. Oh, I.W. Lyo, Surf. Coat. Technol. 200 (2005) 1248–1251.
- [31] Z. Yang, G. Xia, X. Li, J.W. Stevenson, Int. J. Hydrogen Energy 32 (2007) 3648–3654.
- [32] C.C. Mardare, M. Spiegel, A. Savan, A. Ludwig, J. Electrochem. Soc. 156 (2009) B1431–B1439.
- [33] J. Wu, Y. Jiang, C.D. Johnson, X. Liu, J. Power Sources 177 (2008) 365–376.
- [34] J. Wu, C.D. Johnson, Y. Jiang, R.S. Gemmena, X. Liu, Electrochim Acta 54 (2008) 793–800.
- [35] S. Geng, Y. Li, Z. Ma, L. Wang, L. Li, F. Wang, J. Power Sources 195 (2010) 3256–3260.
- [36] Z. Bi, J. Zhu, J.L. Batey, J. Power Sources 195 (2010) 3605–3611.
- [37] N. Shaigan, W. Qu, D.G. Ivey, W. Chen, J. Power Sources 195 (2010) 1529–1542.
- [38] S. Geng, J. Zhu, M.P. Brady, H.U. Anderson, X. Zhou, Z. Yang, J. Power Sources 172 (2007) 775–781.
- [39] S. Geng, D. Xiang, Y. Li, L. Li, L. Wang, J. Chin. Rare Earth Soc. 28 (2010) 423–426.